New Wang-Landau approach to obtain phase diagrams for multicomponent alloys

Kazuhito Takeuchi, Ryohei Tanaka, and Koretaka Yuge

A new Wang-Landau approach to obtain phase diagrams for multicomponent alloys

Kazuhito Takeuchi, Ryohei Tanaka, and Koretaka Yuge

Department of Materials Science and Engineering,
Kyoto University, Sakyo, Kyoto 606-8501, Japan

(Dated: September 21, 2017)

We develop an approach to apply Wang-Landau algorithm to multicomponent alloys in a semi-grand-canonical ensemble. Although the Wang-Landau algorithm has great advantages over conventional sampling methods, there are few applications to alloys. This is because calculating compositions in a semi-grand-canonical ensemble via the Wang-Landau algorithm requires a multi-dimensional density of states in terms of total energy and compositions, and constructing it is difficult from the viewpoints of both implementation and computational cost. In this study, we develop a simple approach to calculate the alloy phase diagram based on the Wang-Landau algorithm, and show that a number of one-dimensional densities of states could lead compositions in a semi-grand-canonical ensemble as a multi-dimensional density of states could. Finally, we apply the present method to Cu–Au and Pd–Rh alloys and confirm that the present method successfully describes the phase diagram with high efficiency, validity and accuracy.

I. INTRODUCTION

In alloy studies with first-principle calculations, estimating thermodynamic properties such as free energy is a major goal. Thermodynamic integration (TI), which is based on the Metropolis algorithm[1], is one of the most widely-used methods to calculate thermodynamic properties and temperature-composition phase diagrams[2–5]. In simulations on a given lattice, cluster expansion[6] (CE) formalism, which reconstructs the coarse-grained Hamiltonian from the outputs of density functional theory (DFT), plays an important role for alloys[7–9] because CE describes the multibody interactions caused by the metallic bonds. Hence, the combination of DFT, CE and TI has been widely used for estimating alloy phase diagrams.

Although TI is a powerful method to calculate free energy, TI has a significant problem in that it suffers from phase transitions. At 1st-order phase transitions, the tunneling barrier between coexisting phases increases exponentially by the Boltzmann factor. This causes inaccurate estimation of phase transition points and also of the free energies near the transition points. In addition, at 2nd-order phase transitions, critical slowing down also leads to inaccurate results near the transition points. In alloy studies, these problems have been avoided by looking for intersections of free energies between two metastable phases[2–5].

The Wang-Landau (WL) algorithm[10,11] is one of the most efficient and accurate methods to obtain the density of states, characterizing the thermodynamic properties of a considered system at equilibrium. Let us explain the characteristics of the WL algorithm. The partition function, Z, is given as:

$$Z = \sum_E W(E) \exp\left(-\frac{E}{k_{\mathrm{B}}T}\right). \tag{1}$$

Here, $W(E)$ is the density of states (DOS), k_{B} is the Boltzmann constant and T is temperature. Compared with the Metropolis algorithm[1], we emphasize that the disadvantage of the WL algorithm is that the simulation time exhibits power-law scaling for system size[39–41] (see Appendix for further details). Although this poor scaling strongly limits using the WL algorithm for a huge system, there are some important advantages: (i) it overcomes the problems caused by 1st- and 2nd-order phase transitions, (ii) it calculates Helmholtz free energy directly, and (iii) once $W(E)$ is estimated, one can calculate the free energy using Eq. (1) and $F = -k_{\mathrm{B}}T \ln Z$ at any temperatures. These advantages are achieved by a random walker that covers the whole energy space and constructs the $W(E)$ efficiently.

Although the WL algorithm has these great advantages over the conventional method, there are few applications to alloys. This is because canonical WL methods[12,13] where compositions in a given simulation cell are fixed have difficulty describing the phase-separated states. Therefore, for constructing alloy phase diagrams, a semi-grand-canonical ensemble has been used instead of the canonical one, but a multi-dimensional DOS is typically required in the WL scheme. WL studies on a multi-dimensional density of states[14–19] indicated difficulties connecting[20] or interpolating[21] the pieces of $W(E)$. Although the above difficulties have been overcome by tools such as the multi-parallel framework[16–19], constructing a multi-dimensional density of states remains quite a difficult problem because of the associated computational costs. Since all of the bins must satisfy the flatness criterion simultaneously, wasteful accumulations of DOS occur[22] and the simulation time becomes large if the dimension of DOS increase.

In this study, we suggest a new method to construct the phase diagram for multicomponent alloys based on the WL algorithm, avoiding explicit construction of the multi-dimensional DOS but using a number of one-dimensional DOSs in a semi-grand-canonical ensemble. Although many grand-canonical WL methods have been proposed, the semi-grand-canonical one has not been proposed because describing phase-separated states correctly with the CE scheme is a unique problem for alloy

phase diagrams. We applied the present method to two binary alloys, Cu–Au and Pd–Rh, which show ordering and phase-separation tendencies respectively. Through these two alloys, we confirmed that our method successfully calculates their phase diagrams and captures the characteristics of Cu–Au and Pd–Rh. Moreover, even though our method suffers from poor scaling originating from the WL algorithm, we found that this semi-grand-canonical WL method shows weaker scaling than the canonical WL method (see Appendix). Note that there is a great advantage in that our method could be combined with the multi-parallel framework[16–19]. As above, the combination of DFT, CE and WL offers be a promising method to obtain alloy phase diagrams.

II. METHODOLOGY

First, in Sec. II A, we give a brief explanation of CE which describes the total energy of an alloy by the coarse-grained Hamiltonian. Second, in Sec. II B, the conventional WL algorithm in the canonical ensemble for alloys is presented. Finally, in Sec. II C, we show how to apply the conventional WL algorithm to multicomponent alloys, and why the conventional one is not suitable for multicomponent alloys. As above, we present a new method based on the WL algorithm to handle multicomponent alloys.

A. Cluster expansion

In CE, atomic configuration on a given lattice, σ, is described by a complete and orthogonal set of discrete basis functions. Suppose that the occupation of an element on lattice site i is specified by an Ising-like spin variable S_i. CE introduces the cluster on the lattice, k, e.g., points, pairs and triplets. Especially in a binary alloy, if the basis functions on a lattice point, i, are $\{1, S_i\}$ where S_i has +1 or 1, the so-called "correlation function", ξ_k, is defined as the average of products of spin variables on k over all symmetrically equivalent k in σ. Thus, the configurational property, e.g., E, is completely represented via correlation functions and their coefficients:

$$E_{\mathrm{CE}}(\sigma) = \sum_k V_k \xi_k(\sigma), \qquad (2)$$

where V_k is called the effective cluster interaction (ECI) and can be practically obtained by fitting the DFT formation energy. Since in Eq. (2) V_ks are constant and only ξ_ks are variable, the formation energy for any configuration is easily obtained compared with DFT. Thus, this coarse-grained Hamiltonian E_{CE} enables us to calculate the large number of energies that is required for the MC simulations.

B. Wang-Landau algorithm in canonical ensemble

Suppose a random walker exists in a configuration space. If we consider an Ising spin model, the moves of the walker is often defined as single-spin flip, which may change its orientation. However, if we consider an alloy system in a canonical ensemble, single-spin flip method could not be used because the chemical potentials for each element should be considered (unlike in the Ising spin model without a field) and therefore compositions should remain constant. Thus, in order to keep compositions fixed, a pair of spin exchanges, where a pair of spins attempt to exchange their positions, is often used in alloy studies. Through repeated updates of the configuration, one obtains the time series of the random walker corresponding to the samples of configuration. In the Metropolis algorithm, since the acceptance ratio is proportional to $\exp\left(-\frac{E}{k_{\mathrm{B}}T}\right)$, the time series corresponds to the samplings from the canonical distribution.

In the WL algorithm, the acceptance ratio is proportional to $1/W(E)$, enabling the random walker to attain all states uniformly in the energy space. After the acceptance or rejection trial, $W(E)$ is updated as $W(E) \to W(E) \times f$ where f is a modification factor that is initially greater than $f_0 = e^1$. At the same time, the histogram $H(E)$ is also incremented as $H(E) \to H(E) + 1$. When $H(E)$ becomes sufficiently "flat", f is reduced such that $f_{i+1} = \sqrt{f_i}$ and all histogram bins are reset to zero. Although there are many definitions of flatness of $H(E)$[10,11,23,24], in this study we regard $H(E)$ as "flat" when all possible $H(E)$ are larger than 80% of the average of $H(E)$[10,11]. Finally, f becomes sufficiently small (e.g., $f \simeq 10^{-8}$) to stop the simulation because f is relevant to the error of estimated DOS[22].

In order to obtain temperature-composition phase diagrams for alloys, both the free energy and compositions are required at a specific temperature. Under specific compositions in a canonical ensemble, we need only the Helmholtz free energy, which is easily obtained by the estimated DOS. Although the above discussion is theoretically correct, the above canonical method may cause a significant error of the free energy due to practical reasons, using the finite simulation cell. The finite simulation cell under fixed compositions makes the configuration attained a phase-separated mixture, which causes interfacial contributions to total energy. This contribution due to the finite simulation cell produces an inaccurate DOS different from the true DOS in the infinite system, and makes it difficult to describe phase separation. This problem is avoided using a semi-grand-canonical ensemble.

C. Present extension of Wang-Landau algorithm for a semi-grand-canonical ensemble

The semi-grand-canonical (SGC) ensemble has been widely used for estimating phase diagrams of alloys. In an SGC ensemble, concentrations are allowed to vary under externally imposed chemical potentials with a fixed total number of atoms. This is different from a grand-canonical ensemble in which both the concentrations and the total number of atoms vary. One of the advantages of SGC is that the configuration never becomes a phase-separated mixture[2] and always shows a pure phase. Therefore, interfacial contributions from a phase-separated mixture do not contribute to the calculated thermodynamic properties in the SGC ensemble and the DOS is estimated within acceptable error in a finite simulation cell.

Hereinafter, for simplicity, we consider an A-B binary alloy without lack of generality. We can thus simply regard the concentration x as $x = x_B$ and the chemical potential μ as $\mu = \mu_B - \mu_A$.

In the SGC ensemble, the corresponding partition function is defined as:

$$Y(T, \mu) = \sum_{E,x} W(E, x) \exp\left(-\frac{E - \mu N x}{k_B T}\right). \quad (3)$$

Unlike in the canonical ensemble where the compositions are obtained trivially, in the SGC ensemble, since we handle chemical potentials instead of compositions, we should calculate ensemble-averaged compositions. A straightforward solution to obtain the compositions in the SGC ensemble is

$$\langle x \rangle = \frac{\sum_{E,x} x W(E, x) \exp\left(-\frac{E - \mu N x}{k_B T}\right)}{Y(T, \mu)}. \quad (4)$$

Here $\langle \rangle$ denotes the ensemble average and N denotes the system size. Eq. (4) means that calculating phase diagrams for a multicomponent alloy requires a multi-dimensional DOS in terms of total energy and compositions. Here again, the difficulties for calculating a multi-dimensional DOS are too time-consuming to construct the DOS[22] compared to a one-dimensional DOS and errors arise in connecting[20] or interpolating[21] the pieces of DOS. In order to avoid these difficulties, we suggest using the thermodynamic relation.

If we consider μ as constant, the total energy in Eq. (2) is rewritten as:

$$\hat{E} = E - \mu N x. \quad (5)$$

Then Eq. (3) is rewritten as:

$$Y(T, \mu) = \sum_{\hat{E}} W_\mu(\hat{E}) \exp\left(-\frac{\hat{E}}{k_B T}\right). \quad (6)$$

The thermodynamic potential in the SGC ensemble, ϕ, is derived from $\phi(T, \mu) = -k_B \ln Y$, like the Helmholtz
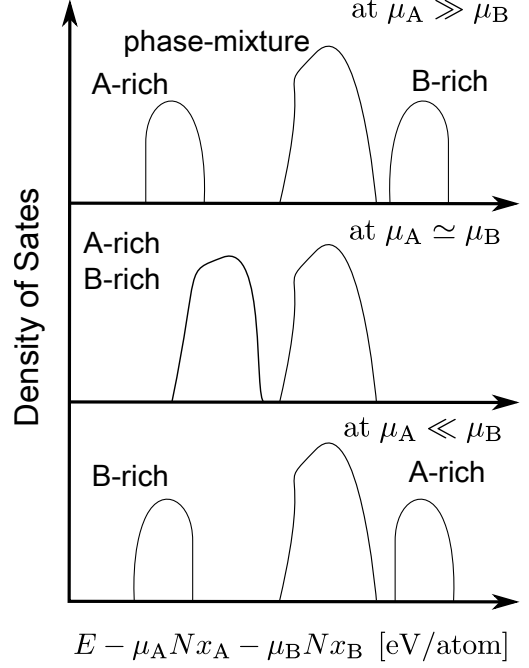

FIG. 1. Schematic illustration of the the DOS for binary phase-separation alloy under three types of chemical potential.

free energy in the canonical ensemble. Otherwise, the ensemble averaged composition could not be calculated through Eq. (6) because $W_\mu(\hat{E})$ is not a function of x. Here, ϕ has a relationship to F through the Legendre transformation:

$$\phi = F - \mu N x. \quad (7)$$

We can obtain x using partial differentiation through interpolating ϕ for each chemical potential:

$$x = -\frac{\partial \phi}{\partial(\mu N)}. \quad (8)$$

Here we offer a qualitative discussion as to why this sampling method gives a desirable result, although our method samples all phase-separated mixtures including interfacial energy like the canonical method samples. In Fig. 1, we show a schematic illustration of the DOS for a binary phase-separation alloy under three types of chemical potential. Under any condition $\mu_A \gg \mu_B$, $\mu_A \ll \mu_B$ or $\mu_A \simeq \mu_B$, the A-rich or B-rich phase shows low energy compared to phase-separated mixtures including high interfacial energy. Since the contribution of high energy DOS to free energy will vanish at low temperature where the phases are separated, phase-separated mixtures do not affect free energy in the semi-grand-canonical method. Obtaining a desirable result, which means the free energy free from undesirable interfacial energy, mainly depends on whether the low energy DOS

is correctly described or not. This restriction, which originates from using the finite simulation cell, affects the free energy and leads to undesirable results. (This undesirable result is demonstrated in Sec. III B.) From this simple discussion, the semi-grand-canonical WL method, which completely samples each low-energy states and phase-separated mixtures, could appropriately describe the free energy and equilibrium state.

Here we summarize two advantages of our method over the canonical method. The primary advantage over the multi-dimensional one that not all the information of DOS is needed. Even if one would like to obtain a partial phase diagram, the conventional WL algorithm should be constructed for whole of the multi-dimensional DOS to calculate Eq. (4). In contrast, our method needs a number of one-dimensional DOSs only near the target region. Even though many $W_\mu(\hat{E})$ are required for Eq. (8), the total simulation time is much shorter than that of $W(E, x)$ because again our method explicitly avoid wasteful accumulations in matching the pieces of DOS. The Secondary advantage is that our method uses a single-spin-flip method instead of a pair of spin exchanges because our method does not fix the compositions. Comparing the two types of updated methods, we discuss the simulation time requirements and limitations of our method in Appendix V.

FIG. 2. ECI for (a) Cu–Au and (b) Pd–Rh alloys except for empty cluster ECI. Broken line indicates zero.

III.   RESULTS AND DISCUSSION

In order to confirm validity and applicability of our method, we applied it to Cu–Au (Sec. III A) and Pd–Rh (Sec. III B) alloys.   Cu–Au alloy shows a 1st order-disorder phase transition, and has been quite well studied[25–28] in terms of experiments and first-principles calculations. Through its application to Cu–Au, we confirmed that our method could describe the ordering tendency of alloys. Pd–Rh alloy, on the other hand, shows a phase-separation tendency where two phases coexist. We also applied our method to Pd–Rh alloy in order to confirm that it can describe the phase coexistence, Pd–Rh is also quite a well-studied system[29–31].

Note that in this study, for simplicity, we only consider the configurational free energy, and do not include non-configurational free energies, e.g., vibrational and electronic free energy. Although, in general, the vibrational effect is significant for phase diagrams especially in ordering alloys, it just lowers the transition temperatures and does not change the low-temperature phases in Cu–Au[28]. Therefore, even by considering only the configurational free energy, we can capture the characteristics for ordering tendency and the phase diagrams of Cu–Au and phase-separation tendency and phase diagram of Pd–Rh without lack of validity.
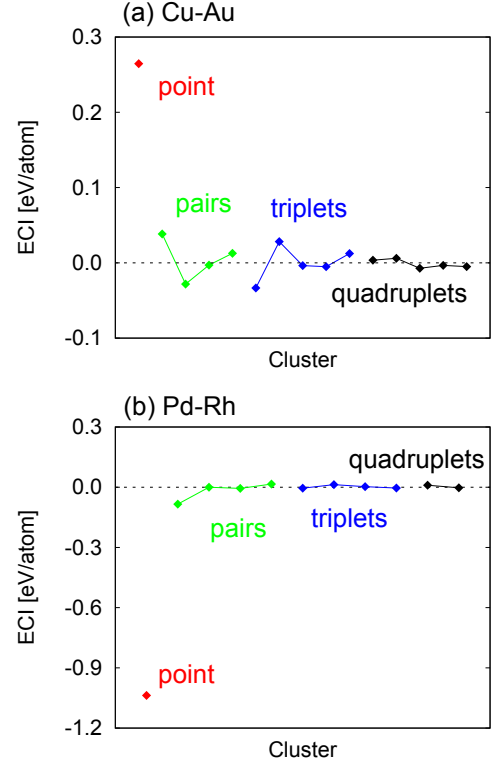
A.   Cu–Au

For the calculation conditions, total energies are obtained by first-principles calculation via the VASP code[32,33], based on the projector-augmented wave method (PAW)[34] within the generalized-gradient approximation of Perdew-Burke-Ernzerhof (GGA-PBE)[35] to the exchange-correlation functional. The plane wave cutoff of 500 eV is used, and atomic positions are fully relaxed on the underlying fcc lattice. Total energies of 183 structures consisting of up 32 atoms are calculated. We obtained 16 optimized ECI (see Fig. 2(a)) with a prediction accuracy, a cross-validation score, of 1.1 meV/atom, which gives sufficient accuracy to capture the thermodynamic characteristics for Cu–Au alloy. In Fig. 2(a), since the nearest neighbor pair ECI has largest positive value, we can see a strong tendency to order. The triplet and quadruplet ECIs, which mainly mean a contribution of atomic local relaxation, are large because there are large differences in lattice constant between Cu and Au. In Fig. 3, through using derivative structures[36] up to 12 atoms, we checked whether our ECIs are valid for describing $L1_0$ at $Cu_{0.5}Au_{0.5}$ and $L1_2$ at $Cu_{0.75}Au_{0.25}$ and $Cu_{0.25}Au_{0.75}$, and confirmed that our ECI completely describes the low temperature phases in Cu–Au.

The simulations were done for a $4 \times 4 \times 4$ supercell on fcc until the factor reached $f_{final} \leq \exp(10^{-7})$. For each simulation, we set the chemical potential $\mu =$
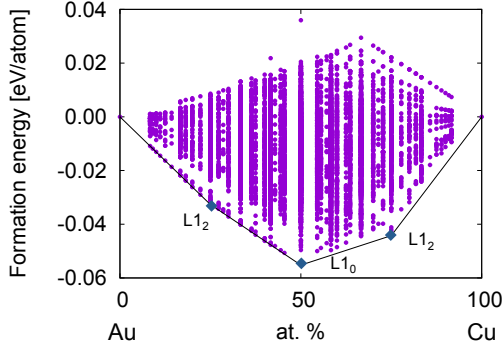
FIG. 3. Formation energies obtained via all derivative structures up to 12 atoms, 10850 structures.
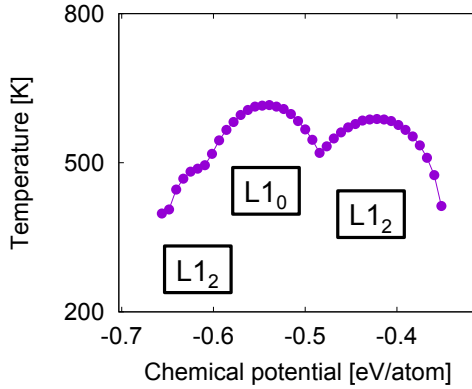

FIG. 4. Cu–Au T-μ phase diagram. Points denote highest heat capacities for each chemical potential. Note that two metastable states coexist at any phase transition point in the T-μ phase diagram, unlike in the T-x one.
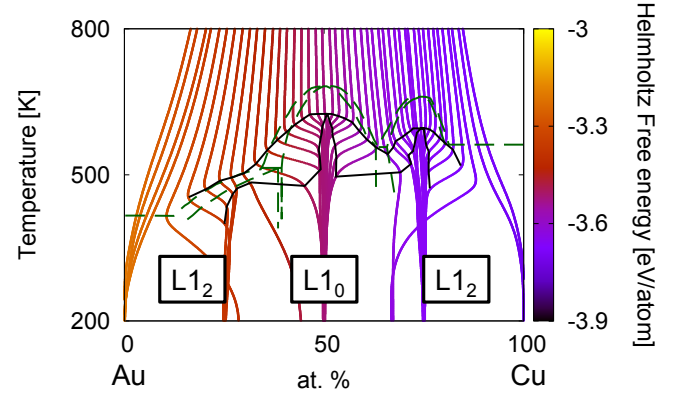

FIG. 5. Cu–Au Helmholtz free energies and compositions obtained by our method over the range from 200K to 800K. Solid line denotes the order-disorder phase transition temperatures obtained by the T-μ phase diagram in Fig. 4 and Eq. (8). Broken line indicates experimental results[37].

and the small size of our simulation cell. As above, our method is found to be applicable to an alloy which shows an ordering tendency.

B. Pd–Rh

The calculation conditions for Pd–Rh are almost same as that for Cu–Au in Sec. III A. The differences are as follows; the plane wave cutoff of 600 eV is used and total energies of 71 structures consisting of up 32 atoms are calculated. We obtained 12 optimized ECI (see Fig. 2(b)) with a cross-validation score of 0.8 meV/atom, which gives sufficient accuracy to describe the phase-separation tendency for Pd–Rh alloy. In Fig. 2(b), since the nearest neighbor pair ECI has the largest negative value, we can see a strong tendency to separate. The triplet and quadruplet ECIs are small because there are only small differences in lattice constant between Pd and Rh.

The simulations were performed for $6 \times 6 \times 6$ supercells on fcc until the factor reached $f_{final} \leq \exp(10^{-7})$. For each simulation, we set the chemical potential $\mu = \mu_{Rh} - \mu_{Pd} = (\text{-}2.079)\text{-}(\text{-}2.043)$ eV/atom.

The temperature-composition phase diagram for Pd–Rh is shown in Fig. 6 with the same procedure as for Cu–Au. Unlike Cu–Au, which shows a 1st-order phase transition, the phase-separation system does not always show a clear peak of heat capacity under a specific μ. However, by comparing the Helmholtz free energy for each phase at a given temperature, we could detect the phase boundary. In Fig. 7, the Helmholtz free energy at $T = 900$K is shown with a linear transformation for the sake of clarity. With least-squares fitting to a quadratic curve for each phase, we can clearly see a common tangent line between the two curves indicating phase coexistence at a specific T and μ. Regarding the phase boundary as the points of contact between the quadratic curves and the cotangent

$\mu_{Au} - \mu_{Cu} = 0.313\text{-}0.703$ eV/atom, and calculated $\phi(T, \mu)$ using $W_\mu(\hat{E})$ and Eq. (6). In Fig. 4, we plot the T-μ phase diagram where a phase transition point is regarded as one that shows the highest heat capacity, $C_{max}(T, \mu)$. We confirmed three order phases in Cu–Au, $L1_0$ for $Cu_{0.5}Au_{0.5}$ and $L1_2$ for both $Cu_{0.75}Au_{0.25}$ and $Cu_{0.25}Au_{0.75}$ through the whole of simulation.

The temperature-composition phase diagram for Cu–Au by our method is shown in Fig. 5. This phase diagram is obtained by converting the T-μ phase diagram (Fig. 4) into a T-x one (Fig. 5) through Eq. (8) with the interpolation of $\phi(T, \mu)$ for each chemical potential via a cubic spline function. Note that two phases are in equilibrium at a specific phase transition point in the T-μ phase diagram. Therefore, we consider one phase as one just before phase transition and another as just after that. Comparing our results and the experimental data[37], we confirmed that our method successfully describes the Cu–Au phase diagram capturing the thermodynamic characteristics of Cu–Au alloy. However, we could see that some simulations under a specific μ would fail to describe $F(T, x)$ correctly. This is due to the differential error in Eq. (8)
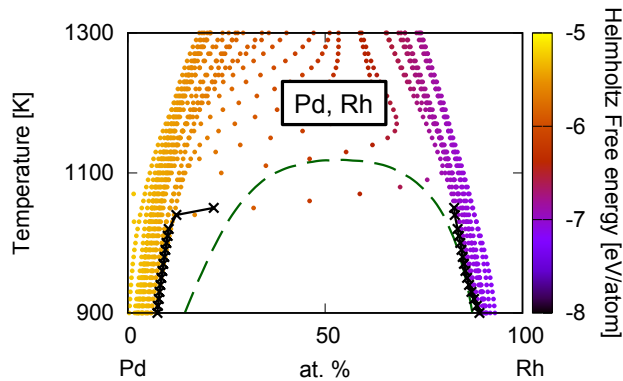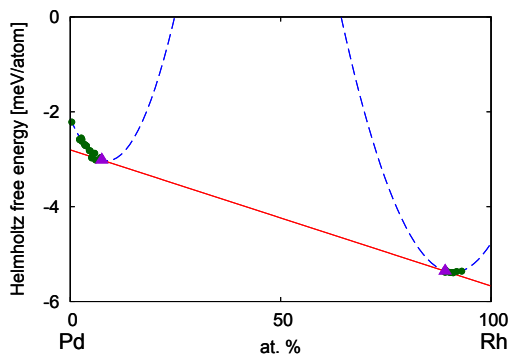
FIG. 6. Pd–Rh Helmholtz free energies and compositions obtained by our method over the range from 900K to 1300K. Solid line denotes the phase-separation line obtained by our method. Broken line indicates experimental results[38].
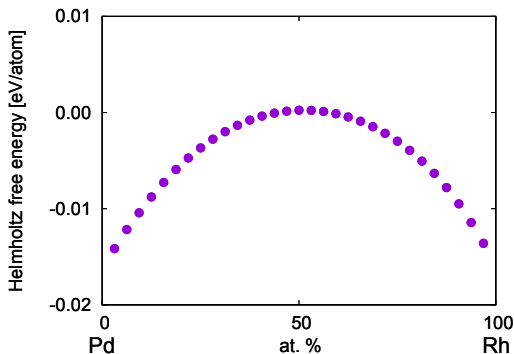

FIG. 7. (a) Closed circle points denote the Pd–Rh Helmholtz free energy at 900K in Fig. 6. Quadratic curves denote the fitted value of points for each phase. The straight line denotes a common tangent line between the two quadratic curves. Closed triangle points denote the points of contact between the curves and the line. (b) Pd–Rh Helmholtz free energy at 900 [K].

line, we could explicitly detect the phase boundary for Pd–Rh shown as a solid line in Fig. 6.

IV. SUMMARY

We suggest a new approach to obtain temperature-composition phase diagrams for multicomponent alloys using the Wand-Landau algorithm. Since our method is not affected by 1st- and 2nd-order phase transitions, we can calculate the phases and free energies with high accuracy even near phase transition points where the Metropolis algorithm and thermodynamic integration lose accuracy. Through the application of our method to Cu–Au and Pd–Rh, we successfully obtained the phase diagrams and free energies. This new approach can replace the multi-dimensional DOS as a number of one-dimensional DOSs also improves the computational efficiency for estimating alloy phase diagrams.

V. APPENDIX

In this section, two types of update scheme are compared, i.e., single-spin-flip (SSF) in the semi-grand-canonical ensemble and pair-atoms-exchange (PAE) in the canonical ensemble. The performance of simulation methods has been measured by the average tunneling time[39–41], τ, defined as the number of MC steps that a random walker takes from a ground state to an anti-ground state (or vice versa). It has been reported[39] that τ for a two-dimensional square lattice $L \times L$ Ising model exhibits power-law scaling, $\tau \propto L^{2d+z}$, by the perfect flat-histogram method based on the exact density of states. Here z is a scaling parameter that depends on the system. The exact DOS for the $L \times L$ Ising model with SSF has been clarified[42], while that with PAE under equiatomic compositions has been not. In order to compare with two update types on the same scheme, we use the estimated DOS by $f \simeq 10^{-8}$ and 90% flatness criterion. Note that even if the ground states are the same between ensembles, the ensembles are naturally different in the simulation. However, both of them become equivalent theoretically when the system size is infinite. Thus, this comparison would be rationalized if the two types of the update scheme exhibit the same time-scaling through several finite simulation cells for $L = 4, 8, 16, 32$. Besides,
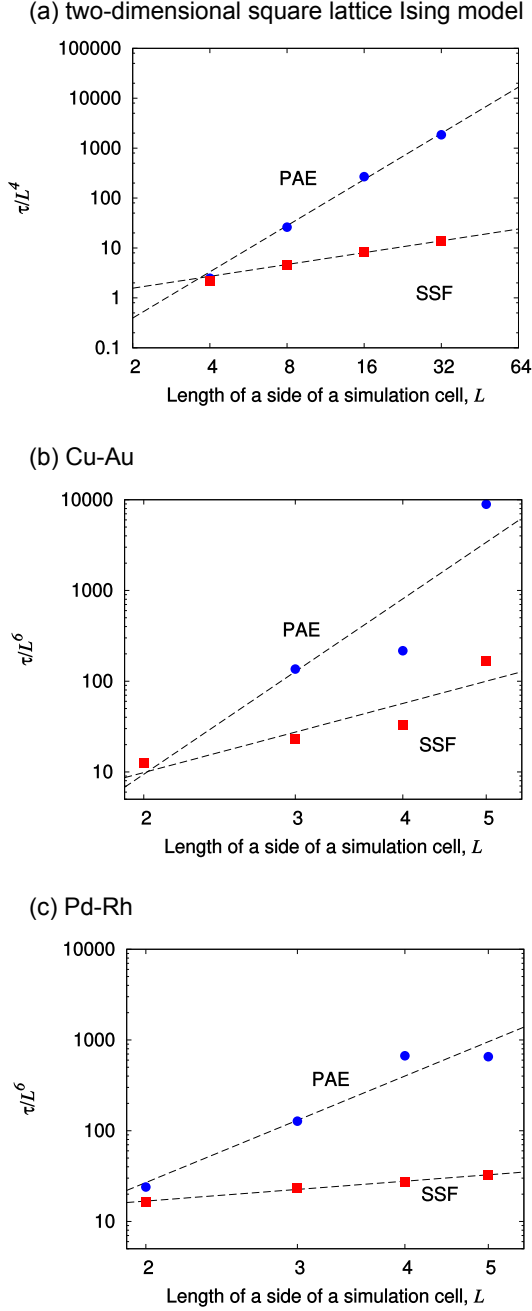
FIG. 8. Scaling of average tunneling times τ using single-spin-flip (SSF) and pair-atoms-exchange (PAE) method for (a) two-dimensional square lattice Ising model, (b) Cu–Au and (c) Pd–Rh. Closed circles and squares denote τ_{PAE} and τ_{SSF} respectively. Broken lines are fitted to each result, and their slope corresponds to z.

it is interesting to show tunneling times for $L \times L \times L$

Cu–Au and Pd–Rh ($L = 2, 3, 4, 5$).

In Fig. 8, the results of τ_{SSF} and τ_{PAE} are plotted and fitted as linear functions in terms of L. Fig. 8 shows that τ_{PAE} also exhibits the power-law scaling with high z, like τ_{SSF}. In Table I, we show the scaling parameters z obtained by fitting the tunneling times. The large

TABLE I. Scaling parameter z for two-dimensional square lattice Ising model (2D Ising), Cu–Au and Pd–Rh by single-spin-flip (SSF) and pair-atoms-exchange (PAE).

	z_{SSF}	z_{PAE}
2D Ising	0.788 ± 0.029	3.073 ± 0.165
Cu–Au	2.529 ± 0.838	6.423 ± 1.713
Pd–Rh	0.728 ± 0.049	3.899 ± 0.670

difference between z_{SSF} and z_{PAE} is due to the ratio of $\rho(E_1)/\rho(E_0)$ where $\rho(E_0)$ is the number of ground states and $\rho(E_1)$ is the number of first exited states. Although $E_0^{\mathrm{SSF}} = E_0^{\mathrm{PAE}}$ and $\rho_{\mathrm{SSF}}(E_0) = \rho_{\mathrm{PAE}}(E_0)$, there is a large difference in the ratio:

$$\frac{\rho_{\mathrm{SSF}}(E_1^{\mathrm{SSF}})}{\rho(E_0)} \propto N,$$

$$\frac{\rho_{\mathrm{PAE}}(E_1^{\mathrm{PAE}})}{\rho(E_0)} \propto N^2.$$

The difference of z between PAE and SSF for the Ising model, $\Delta z^{\mathrm{Ising}} \simeq= \tau_{\mathrm{PAE}} - \tau_{\mathrm{SSF}} = 2.285$, is in good agreement with this ratio difference $N = L^2$ due to the simplicity of the model. Likewise, although the results for CuAu and PdRh include errors in $L = 4, 5$ due to the complexity of their models, $\Delta z^{\mathrm{CuAu}} \simeq 3.894$ and $\Delta z^{\mathrm{PdRh}} \simeq 3.171$ also show the tendency with the ratio difference $N = L^3$.

Here we summarize the disadvantages and advantages of our method (semi-grand-canonical WL method) compared with the canonical WL method. Except for the condition that a system shows an ordering tendency under specific dilute compositions (i.e., the ground state is not described as a phase-separated mixture state and the number of possible states the simulation attains under specific compositions is considerably smaller than that under not composition restriction), the above discussion indicates that in alloy studies our method based on a semi-grand-canonical ensemble is generally useful for not only estimating accurate thermodynamic properties but also for searching for the ground state structure, which is difficult for the canonical WL method.

[1] N. Metropolis, A. W. Rosenbluth, M. N. Rosenbluth, A. H. Teller, and E. Teller, The Journal of Chemical Physics **21**, 1087 (1953).

[2] A. van de Walle and M. Asta, Modelling and Simulation

in Materials Science and Engineering **10**, 521 (2002).

[3] A. van de Walle and G. Ceder, Journal of Phase Equilibria **23**, 348 (2002).

[4] A. van de Walle, M. Asta, and G. Ceder, Calphad **26**, 539 (2002).

[5] A. van de Walle, Calphad **33**, 266 (2009), tools for Computational Thermodynamics.

[6] J. M. Sanchez, F. Ducastelle, and D. Gratias, Physica A: Statistical Mechanics and its Applications **128**, 334 (1984).

[7] B. Puchala and A. Van der Ven, Phys. Rev. B **88**, 094108 (2013).

[8] A. V. Ruban and I. A. Abrikosov, Reports on Progress in Physics **71**, 046501 (2008).

[9] A. Van der Ven and G. Ceder, Phys. Rev. B **71**, 054102 (2005).

[10] F. Wang and D. P. Landau, Phys. Rev. Lett. **86**, 2050 (2001).

[11] F. Wang and D. P. Landau, Phys. Rev. E **64**, 056101 (2001).

[12] M. Borg, C. Stampfl, A. Mikkelsen, J. Gustafson, E. Lundgren, M. Scheffler, and J. N. Andersen, ChemPhysChem **6**, 1923 (2005).

[13] S. N. Khan and M. Eisenbach, Phys. Rev. B **93**, 024203 (2016).

[14] C. Zhou, T. Schulthess, S. Torbrügge, and D. Landau, Phys. Rev. Lett. **96** (2006), 10.1103/PhysRevLett.96.120201.

[15] S. Tsai, F. Wang, and D. Landau, Braz J Phys **38**, 6 (2008).

[16] T. Vogel, Y. Li, T. Wüst, and D. Landau, Phys. Rev. Lett. **110** (2013), 10.1103/PhysRevLett.110.210603.

[17] Y. Li, T. Vogel, T. Wüst, and D. Landau, J. Phys.: Conf. Ser. **510**, 012012 (2014).

[18] T. Vogel, Y. Li, T. Wüst, and D. Landau, J. Phys.: Conf. Ser. **487**, 012001 (2014).

[19] T. Vogel, Y. Li, T. Wüst, and D. Landau, Phys. Rev. E **90** (2014), 10.1103/PhysRevE.90.023302.

[20] S.-H. Tsai, F. Wang, and D. P. Landau, Brazilian Journal of Physics **38**, 6 (2008).

[21] K. Sato, S. Takizawa, and T. Mohri, Journal of the Physical Society of Japan **79**, 084602 (2010), http://dx.doi.org/10.1143/JPSJ.79.084602.

[22] C. Zhou and R. N. Bhatt, Phys. Rev. E **72**, 025701 (2005).

[23] R. E. Belardinelli and V. D. Pereyra, Phys. Rev. E **75**, 046701 (2007).

[24] M. S. Shell, P. G. Debenedetti, and A. Z. Panagiotopoulos, Phys. Rev. E **66**, 056703 (2002).

[25] V. Ozoliņš, C. Wolverton, and A. Zunger, Phys. Rev. B **57**, 6427 (1998).

[26] Z. W. Lu, S.-H. Wei, A. Zunger, S. Frota-Pessoa, and L. G. Ferreira, Phys. Rev. B **44**, 512 (1991).

[27] S. H. Wei, A. A. Mbaye, L. G. Ferreira, and A. Zunger, Phys. Rev. B **36**, 4163 (1987).

[28] V. Ozoliņš, C. Wolverton, and A. Zunger, Phys. Rev. B **58**, R5897 (1998).

[29] P. E. A. Turchi, G. M. Stocks, W. H. Butler, D. M. Nicholson, and A. Gonis, Phys. Rev. B **37**, 5982 (1988).

[30] Z. W. Lu, S.-H. Wei, and A. Zunger, Phys. Rev. Lett. **66**, 1753 (1991).

[31] P. E. A. Turchi, V. Drchal, and J. Kudrnovský, Phys. Rev. B **74**, 064202 (2006).

[32] G. Kresse and J. Hafner, Phys. Rev. B **47**, 558 (1993).

[33] G. Kresse and J. Furthmüller, Phys. Rev. B **54**, 11169 (1996).

[34] G. Kresse and D. Joubert, Phys. Rev. B **59**, 1758 (1999).

[35] J. P. Perdew, K. Burke, and M. Ernzerhof, Phys. Rev. Lett. **77**, 3865 (1996).

[36] G. L. W. Hart and R. W. Forcade, Phys. Rev. B **77**, 224115 (2008).

[37] H. Okamoto, D. J. Chakrabarti, D. E. Laughlin, and T. B. Massalski, *Binary Alloy Phase Diagrams*, Vol. 1 (ASM International) pp. 358–362.

[38] H. Okamoto, D. J. Chakrabarti, D. E. Laughlin, and T. B. Massalski, *Binary Alloy Phase Diagrams*, Vol. 3 (ASM International) pp. 3037–3038.

[39] P. Dayal, S. Trebst, S. Wessel, D. Würtz, M. Troyer, S. Sabhapandit, and S. N. Coppersmith, Phys. Rev. Lett. **92**, 097201 (2004).

[40] S. Trebst, D. A. Huse, and M. Troyer, Phys. Rev. E **70**, 046701 (2004).

[41] M. S. Shell, P. G. Debenedetti, and A. Z. Panagiotopoulos, The Journal of Physical Chemistry B **108**, 19748 (2004), http://dx.doi.org/10.1021/jp047677j.

[42] P. D. Beale, Phys. Rev. Lett. **76**, 78 (1996).